Advances in Aircraft and Spacecraft Science, *Vol. 10, No. 5 (2023) 419-437*
https://doi.org/10.12989/aas.2023.10.5.419

Aeroelastic stability analysis of a two-stage axially deploying telescopic wing with rigid-body motion effects

Sayed Hossein Moravej Barzani* and Hossein Shahverdi[a]

Department of Aerospace Engineering, Amirkabir university of Technology, Tehran, Iran

(Received May 2, 2023, Revised September 25, 2023, Accepted November 13, 2023)

Abstract. This paper presents the study of the effects of rigid-body motion simultaneously with the presence of the effects of temporal variation due to the existence of morphing speed on the aeroelastic stability of the two-stage telescopic wings, and hence this is the main novelty of this study. To this aim, Euler-Bernoulli beam theory is used to model the bending-torsional dynamics of the wing. The aerodynamic loads on the wing in an incompressible flow regime are determined by using Peters' unsteady aerodynamic model. The governing aeroelastic equations are discretized employing a finite element method based on the beam-rod model. The effects of rigid-body motion on the length-based stability of the wing are determined by checking the eigenvalues of system. The obtained results are compared with those available in the literature, and a good agreement is observed. Furthermore, the effects of different parameters of rigid-body such as the mass, radius of gyration, fuselage center of gravity distance from wing elastic axis on the aeroelastic stability are discussed. It is found that some parameters can cause unpredictable changes in the critical length and frequency. Also, paying attention to the fuselage parameters and how they affect stability is very important and will play a significant role in the design.

Keywords: aeroelastic stability; morphing aircraft; rigid body motion; two-stage; variable span wing

1. Introduction

In recent years, morphing wing aircrafts have become a special topic of interest to researchers. Among the various concepts of morphing, the wing deployment concept has been shown to be an effective concept for improving both aircraft range and endurance (Friswell and Inman 2006). However, due to changes in system dynamics by changing the wing dimensions, the flutter prediction is of paramount importance for the analysis and design of an axially deploying telescopic wing**.**

Due to the dimensions and nature of UAV wings, the dynamics of slender wings are mainly modeled with the beam theory (Bisplinghoff *et al.* 2013). Many researchers have modelled the dynamic behaviour of axially deploying telescopic beams. Wang and Wei (1987) modelled the vibration of a robot arm of a moving slender prismatic beam. In this study, it was shown that the length changing of the flexible arm has stabilizing or destabilizing effects on the vibrations of arm. Stylianou and Tabarrok (1994a) studied the axially deploying beam based on finite element

*Corresponding author, Ph.D., E-mail: moravejhossein@aut.ac.ir
[a]Associate Professor, E-mail: h_shahverdi@aut.ac.ir

http://www.techno-press.org/?journal=aas&subpage=7 ISSN: 2287-528X (Print), 2287-5271 (Online)

analysis. This study was then continued by considering the effects of, tip support, tip mass, physical damping, and wall flexibility on the beam stability characteristics using the eigenvalue analysis (Stylianou and Tabarrok 1994b). The eigenvalue analysis was also used to determine the stability of the beam with the constant extension speed based on the Rayleigh beam theory by Chang *et al.* (2010). They also used Floquet theory to investigate the beam stability with motion of periodical back-and-forth. Raftoyiannis and Michaltsos (2013) used a technique of modal superposition for the telescopic cranes' boom dynamic analysis based on a continuum approach. Park *et al.* (2013) determined the dynamic behaviour of an axially deploying telescopic beam modelled by employing the nonlinear theory of von Kármán (Salami and Dariushi 2018). The results showed that the response of the system was consistent for both nonlinear and linear conditions. Furthermore, it was obtained that depending on the Young's modulus and morphing acceleration values, the differences between nonlinear and linear solutions might increase. Duan *et al.* (2014) studied the dynamic response of an axially deploying nested beam experimentally and theoretically. The governing equations of motion were driven employing D'Alembert's principle and a good agreement between numerical and experimental results were obtained. The moving mass effects on the dynamic behavior of a two-stage telescopic mechanism employed in truss structures of a bridge inspection vehicle were investigated by Sui *et al.* (2015). In this research, Euler-Bernoulli beam theory was used to model the structural dynamics of the two-stage telescopic mechanism. This study was then continued to consider the dynamic behavior of a 2-DOF telescopic mechanism (Sui *et al.* 2016b). Yang *et al.* (2016) studied the invariants and energetics of the moving beam with given initial conditions by the method of assumed-mode. It was concluded that when the moving beam is being extended with constant speed, the adiabatic invariant may be kept constant.

As it was mentioned above, the structural dynamics of the span morphing beam depends on its length, and hence the aeroelastic analysis of morphing wings can also be affected. Huang and Qiu (2013) studied the effects of span morphing speeds on the flutter instability of a single variable-span with uniformity assumption (uniform time invariant parameters). They combined Euler-Bernoulli beam theory with an unsteady vortex lattice aerodynamic theory and showed that using a span morphing mechanism can improve the wing aeroelastic performance. Yang and Zhang (2014) investigated the nonlinear vibrations of an axially deploying beam by considering the coupling of the transversal and longitudinal motion. Also, Zhang *et al.* (2014) studied the nonlinear dynamics of a moving orthotropic composite rectangular plate with third-order nonlinear piston and Reddy's third-order plate Theories. It was shown that damping coefficients and deploying speed have special effects on the system stability. This study was then continued to consider the subsonic airflow by combining Kutta-Joukowski lift theorem and von Kármán theory (Zhang *et al.* 2017). They investigated the effects of deploying speed on the nonlinear dynamic behaviour and stability of the system. Huang *et al.* (2018) investigated the aeroelastic response of span-morphing wings with rigid-body motions. The established aeroelastic model was based on Euler-Bernoulli beam theory and unsteady strip aerodynamic theory. It was shown that the quasi static stability of the morphing wing is dependent on the flexibility of fuselage. Research related to the work of Huang *et al.* Includes the works of Schmidt *et al.* (2016)., in which a significant coupling between rigid-body and elastic degrees of freedom on a simple wing is shown (Schmidt 2016). The aeroelastic behavior of a span-morphing wing in supersonic flow employing the piston theory was investigated by Li and Jin (2018). Ajaj and Friswell (2018) considered the sensitivity of the aeroelastic stability of a single variable-span morphing wing for various morphing speeds and system parameters with uniformity assumption. They combined the torsional and bending shape

functions with the Theodorsen's unsteady aerodynamic model, and showed that the wing morphing speed affects the flutter instability of the system, and needs to be taken into account. Ajaj *et al.* (2019) studied the quasi static aeroelastic behaviour of multi-segment, telescopic, stepped, span morphing wing. In this study, Theodorsen's unsteady aerodynamic model and Euler-Bernoulli beam theory were used to form the aeroelastic equations and the effect of morphing speed was ignored. It was concluded that this mechanism can be employed as a means for flutter suppression of the wing. Moravej Barzani *et al.* (2022b) investigated the aeroelastic stability of a two-stage axially moving telescopic wing. The established aeroelastic model was based on Peters' unsteady aerodynamic model (Peters *et al.* 1995) and Euler-Bernoulli beam theory. It was shown that the flutter instability of an axially telescopic wing is more sensitive to the fixed part parameters than the moving part. This study was then continued to consider the effect of structural nonlinearity on the aeroelasticity of span morphing telescopic wings employing the geometrically exact fully intrinsic equations (Moravej Barzani *et al.* 2022a). It was concluded that by using the geometrically exact fully intrinsic equations, the flutter instability of the telescopic morphing wing can be determined more accurately and also the overlapping mass and morphing length have significant effects on the flutter instability of the span morphing telescopic wing. Shafaghat *et al.* (2022) studied the effects of the amount of the bending and the torsional rigidity of the fuselage on the flutter instability. They showed that when the amount of the bending and the torsional rigidity of the fuselage is close to the amounts of the wings and tails, a full aircraft analysis is necessary.

In the present study, the effects of rigid-body motion on the aeroelastic stability of a two-stage axially deploying telescopic wing are investigated. To this aim, Euler-Bernoulli beam theory is used to model the bending-torsional dynamics of the wing, and Peters' unsteady aerodynamic model (Peters *et al.* 1995) is used to simulate the aerodynamic loads. The governing aeroelastic equations are discretized employing a finite element method based on the beam-rod model. Finally, the effects of rigid-body motion on the length-based (Moravej Barzani *et al.* 2022b) stability of the wing is determined by checking the system eigenvalues. It is noted that in none of the previous studies that have observed the rigid-body effects, the morphing speed was used for the aeroelastic analysis of telescopic morphing wings, and hence this is the main purpose and the main novelty of this study. Moreover, the main novelties of this paper are to investigate the effects of rigid-body motion simultaneously with the presence of the effects of temporal variation due to the existence of morphing speed on the aeroelastic stability of two-stage telescopic wing.

2. Governing equations

As shown in Fig. 1, a model of two-stage Euler-Bernoulli beam is used to simulate the structural dynamics of an axially deploying telescopic wing with sliding motion. The wing has a constant morphing speed (constant axially moving speed) of $\dot{\kappa}$, and the length of the moving and fixed parts are denoted by l_m and l_1, respectively. The total time-dependent length, l, can be expressed as

$$l(t) = \dot{\kappa}t + l_1 \tag{1}$$

It should be noted that the range of $l(t)$ has a lower limit of the length of the fixed part and an upper limit of the sum of the length of the fixed part and the increase in length. On the other hand, m_F, x_F and r_F are half of the mass of the fuselage, the fuselage center of gravity distance from wing elastic axis and the radius of gyration of the fuselage, respectively. Also, the fuselage mass

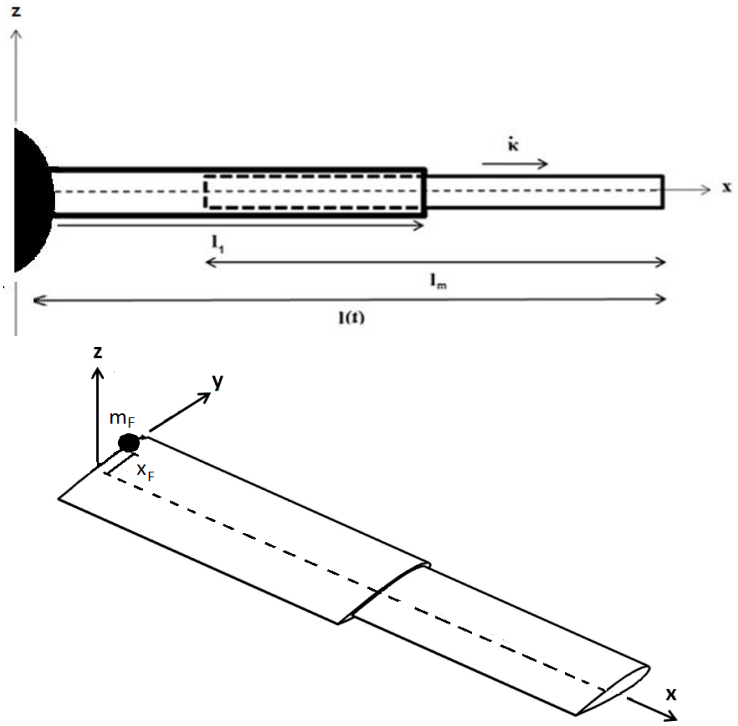

Fig. 1 Two-stage telescopic beam

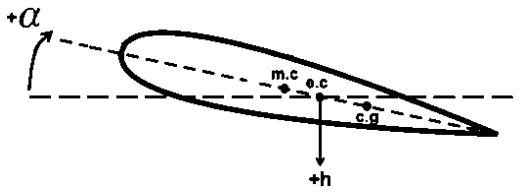

Fig. 2 Typical section of wing

moment of inertia is considered around the *x* axis (pitch motion).

The governing equations of motion are derived employing the extended Hamilton's principle as follows

$$\delta \int_{t_1}^{t_2} (T - V + W) dt = 0 \tag{2}$$

where T, W and V are the kinetic energy, nonconservative work and potential (strain) energy, respectively.

Fig. 2 shows the out-of-plane bending (h) and the torsion (α) degrees of freedom of a typical section of the wing.

The potential and kinetic energies of the wing can be expressed as

$$T = \frac{1}{2}\int_0^{l_1} m_1 \left[\left(\frac{dh_1}{dt} + r_1 \frac{d\alpha_1}{dt}\right)^2\right] dx + \frac{1}{2}\int_{l_1}^{l} m_2 \left[\left(\frac{dh_2}{dt} + r_2 \frac{d\alpha_2}{dt}\right)^2 + \dot{\kappa}^2\right] dx + \frac{1}{2}\int_0^{l_1} I_{c.g_1} \left(\frac{d\alpha_1}{dt}\right)^2 dx +$$

$$\frac{1}{2}\int_{l_1}^{l} I_{c.g_2}\left(\frac{d\alpha_2}{dt}\right)^2 dx+\frac{1}{2}m_F\left[\left(\frac{dh_1^0}{dt}+x_F\frac{d\alpha_1^0}{dt}\right)^2\right]+\frac{1}{2}I_{c.g_F}\left(\frac{d\alpha_1^0}{dt}\right)^2$$

$$V=\frac{1}{2}\int_0^{l_1} EI_1\left(\frac{d^2h_1}{dx^2}\right)^2 dx+\frac{1}{2}\int_0^{l_1} GJ_1\left(\frac{d\alpha_1}{dx}\right)^2 dx+\frac{1}{2}\int_{l_1}^{l} EI_2\left(\frac{d^2h_2}{dx^2}\right)^2 dx+\frac{1}{2}\int_{l_1}^{l} GJ_2\left(\frac{d\alpha_2}{dx}\right)^2 dx+$$
$$\int_0^{l_1} m_1 g(h_1+r_1\alpha_1)dx+\int_{l_1}^{l} m_2 g(h_2+r_2\alpha_2)dx$$

$$W=-F_e h_1(l_1,t)-F_e r_1\alpha_1(l_1,t)+Lh_1(x,t)+Lh_2(x,t)+M\alpha_1(x,t)+M\alpha_2(x,t)$$
$$F_e=m_e(t)[g+\ddot{h}_1(l_1,t)+r_1\ddot{\alpha}_1(l_1,t)] \quad (3)$$

where EI is the bending rigidity, m is the mass per length and GJ is the torsional rigidity. Also, g is the acceleration of gravity, r is the distance between the center of mass and the elastic center, $I_{c.g}$ is the moment of inertia about center of mass, M is the aerodynamic moment, L is the aerodynamic force. Furthermore, the indices $(\bullet_1)$ and $(\bullet_2)$ refer to the fixed and moving parts of the wing, respectively. Also, h_1^0 and α_1^0 denote the plunge motion and pitch motion of the fuselage, respectively.

$m_e(t)$ is the equivalent mass (overlapped part mass) at the end of the fixed part due to the incomplete connection of the moving part with the fixed part (Sui *et al.* 2016a)

$$m_e(t)=\frac{m_2[l_1^3-(l(t)-l_m)^3]}{3l_1^2} \quad (4)$$

The first variation of potential and kinetic energies are defined as

$$\int_{t_1}^{t_2}(\delta T)dt=\int_0^{l_1}\int_{t_1}^{t_2} m_1\left[\frac{dh_1}{dt}+r_1\frac{d\alpha_1}{dt}\right]\left[\frac{d(\delta h_1)}{dt}+r_1\frac{d(\delta\alpha_1)}{dt}\right]dtdx+\int_{l_1}^{l}\int_{t_1}^{t_2} m_2\left[\frac{dh_2}{dt}+\right.$$
$$\left.r_2\frac{d\alpha_2}{dt}\right]\left[\frac{d(\delta h_2)}{dt}+r_2\frac{d(\delta\alpha_2)}{dt}\right]dtdx+\int_{l_1}^{l}\int_{t_1}^{t_2} m_2\dot{\kappa}(\delta\dot{\kappa})dtdx+\int_0^{l_1}\int_{t_1}^{t_2} I_{c.g_1}\frac{d\alpha_1}{dt}\frac{d(\delta\alpha_1)}{dt}dtdx+$$
$$\int_{l_1}^{l}\int_{t_1}^{t_2} I_{c.g_2}\frac{d\alpha_2}{dt}\frac{d(\delta\alpha_2)}{dt}dtdx+\int_{t_1}^{t_2} m_F\left[\frac{dh_1^0}{dt}+x_F\frac{d\alpha_1^0}{dt}\right]\left[\frac{d(\delta h_1^0)}{dt}+x_F\frac{d(\delta\alpha_1^0)}{dt}\right]dt+$$
$$\int_{t_1}^{t_2} I_{c.g_F}\left[\frac{d\alpha_1^0}{dt}\right]\left[\frac{d(\delta\alpha_1^0)}{dt}\right]dt$$

$$\int_{t_1}^{t_2}(\delta V)dt=\int_{t_1}^{t_2}\int_0^{l_1} EI_1\left(\frac{d^2h_1}{dx^2}\right)\ \delta\left(\frac{d^2h_1}{dx^2}\right)\ dxdt+\int_{t_1}^{t_2}\int_{l_1}^{l} EI_2\left(\frac{d^2h_2}{dx^2}\right)\ \delta\left(\frac{d^2h_2}{dx^2}\right)\ dxdt+$$
$$\int_{t_1}^{t_2}\int_0^{l_1} GJ_1\left(\frac{d\alpha_1}{dx}\right)\delta\left(\frac{d\alpha_1}{dx}\right)\ dxdt+\int_{t_1}^{t_2}\int_{l_1}^{l} GJ_2\left(\frac{d\alpha_2}{dx}\right)\delta\left(\frac{d\alpha_2}{dx}\right)\ dxdt+\int_{t_1}^{t_2}\int_0^{l_1} m_1 g(\delta h_1+$$
$$r_1\delta\alpha_1)dx+\int_{t_1}^{t_2}\int_{l_1}^{l} m_2 g(\delta h_2+r_2\delta\alpha_2)dx$$

$$\int_{t_1}^{t_2}(\delta W)dt=\int_{t_1}^{t_2}[L(\delta h_1+\delta h_2)+M_{e.c}(\delta\alpha_1+\delta\alpha_2)-\delta(F_e h_1(l_1,t))-\delta(F_e r_1\alpha_1(l_1,t))]\,dt \quad (5)$$

By substituting Eq. (5) in Eq. (2), the general governing equations of motion for a two-stage telescopic wing can be obtained as follows

$$\left.\begin{aligned}&\left(m_1+m_e\delta(x-l_1)\right)\left[\frac{d^2h_1}{dt^2}+g\right]+m_1r_1\frac{d^2\alpha_1}{dt^2}+\frac{d^2}{dx^2}\left(EI_1\frac{d^2h_1}{dx^2}\right)+\\&+m_F\frac{d^2h_1^0}{dt^2}+m_Fx_F\frac{d^2\alpha_1^0}{dt^2}=L\\&I_{e.c_1}\frac{d^2\alpha_1}{dt^2}+m_er_1\delta(x-l_1)\frac{d^2\alpha_1}{dt^2}+m_1r_1\frac{d^2h_1}{dt^2}-\frac{d}{dx}\left(GJ_1\frac{d\alpha_1}{dx}\right)+m_1r_1g+\\&+m_Fx_F\frac{d^2h_1^0}{dt^2}+m_Fr_F^2\frac{d^2\alpha_1^0}{dt^2}=M_{e.c}\end{aligned}\right\}\ 0<x<l_1$$

$$\left.\begin{aligned} m_2\left(\frac{d^2h_2}{dt^2}+g\right)+m_2r_2\frac{d^2\alpha_2}{dt^2}+\frac{d^2}{dx^2}\left(EI_2\frac{d^2h_2}{dx^2}\right)=L \\ I_{e.c_2}\frac{d^2\alpha_2}{dt^2}+m_2r_2\frac{d^2h_2}{dt^2}-\frac{d}{dx}\left(GJ_2\frac{d\alpha_2}{dx}\right)+m_2r_2g=M_{e.c}\end{aligned}\right\} l_1<x<l \tag{6}$$

where $I_{e.c}=I_{c.g}+mr^2$.

As both torsional and bending variables are functions of space and time, and also due to the fact that $\dot{\kappa}=\frac{dl}{dt}=\frac{dx}{dt}$, the partial derivatives of each variable can be obtained as

$$\begin{aligned}\frac{dh}{dt}&=\frac{\partial h}{\partial t}+\dot{\kappa}\frac{\partial h}{\partial x}\\ \frac{d\alpha}{dt}&=\frac{\partial \alpha}{\partial t}+\dot{\kappa}\frac{\partial \alpha}{\partial x}\\ \frac{d^2h}{dt^2}&=\frac{\partial^2 h}{\partial t^2}+2\dot{\kappa}\frac{\partial^2 h}{\partial x\partial t}+\dot{\kappa}^2\frac{\partial^2 h}{\partial x^2}+\ddot{\kappa}\frac{\partial h}{\partial x}\\ \frac{d^2\alpha}{dt^2}&=\frac{\partial^2 \alpha}{\partial t^2}+2\dot{\kappa}\frac{\partial^2 \alpha}{\partial x\partial t}+\dot{\kappa}^2\frac{\partial^2 \alpha}{\partial x^2}+\ddot{\kappa}\frac{\partial \alpha}{\partial x}\end{aligned} \tag{7}$$

Finally, by substituting Eq. (7) in Eq. (6), and considering suitable torsional and bending shape functions ($H^{\alpha}(x)$ and $H^{h}(x)$), the discretized weak form can be obtained (Moravej Barzani *et al.* 2022b) based on Hermitian beam element and Galerkin method (Cook 2007).

The generalized moment and lift applied on the wing ($M^{g}_{e.c}, L^{g}$) are obtained using Peters' unsteady aerodynamic model as follows (Peters *et al.* 1995)

$$\begin{aligned} L&=\pi\rho b^2\left(\ddot{h}+u\dot{\alpha}-ba\ddot{\alpha}\right)+2\pi\rho ub\left(\dot{h}+u\alpha+b\left(\frac{1}{2}-a\right)\dot{\alpha}-\lambda_0\right)\\ M_{e.c}&=M_{\frac{c}{4}}+b\left(\frac{1}{2}+a\right)L\\ M_{\frac{c}{4}}&=-\pi\rho b^3\left(\frac{1}{2}\ddot{h}+u\dot{\alpha}+b(\frac{1}{8}-\frac{a}{2})\ddot{\alpha}\right)\\ \lambda_0&=\frac{1}{2}\sum_{n=1}^{N}b_{\text{inflow}}\lambda_n\\ [A_{\text{inflow}}]\{\dot{\lambda}_n\}+\frac{u}{b}\{\lambda_n\}&=\{C_{\text{inflow}}\}\left[\ddot{h}+u\dot{\alpha}+b(0.5-a)\ddot{\alpha}\right]\end{aligned} \tag{8}$$

where b is the semi-chord, u is the flight speed, a is the nondimensional distance from the elastic center to the mid-chord, ρ is the air density, and the definitions of $[A_{\text{inflow}}]$, $\{C_{\text{inflow}}\}$ and $\{b_{\text{inflow}}\}$ are presented in the work of (Peters *et al.* 1995). Also, α and h consist of two parts, fixed $(\,)_1$ and movable $(\,)_2$. It is noted that the discretized generalized aerodynamic moment and lift equations are given in Appendix A and related matrices obtained from the discretization process based on shape functions ($H^{\alpha}(x)$ and $H^{h}(x)$) are defined in Appendix B.

The boundary conditions at the roots and the tips of the fixed and moving beams based on rigid-body freedom are listed as follows

$$\begin{aligned}\frac{\partial h_1^0}{\partial x}(t)&=0\\ EI_1\frac{\partial^2 h_1}{\partial x^2}(l_1,t)=EI_2\frac{\partial^2 h_2}{\partial x^2}(l_1,t),\ EI_1\frac{\partial^3 h_1}{\partial x^3}(l_1,t)&=EI_2\frac{\partial^3 h_2}{\partial x^3}(l_1,t),\ GJ_1\frac{\partial \alpha_1}{\partial x}(l_1,t)=GJ_2\frac{\partial \alpha_2}{\partial x}(l_1,t)\\ EI_2\frac{\partial^2 h_2}{\partial x^2}(l,t)=0,\quad EI_2\frac{\partial^3 h_2}{\partial x^3}(l,t)&=0,\quad GJ_2\frac{\partial \alpha_2}{\partial x}(l,t)=0\end{aligned} \tag{9}$$

Finally, the compact form of the discretized aeroelastic governing equations can be written as follows

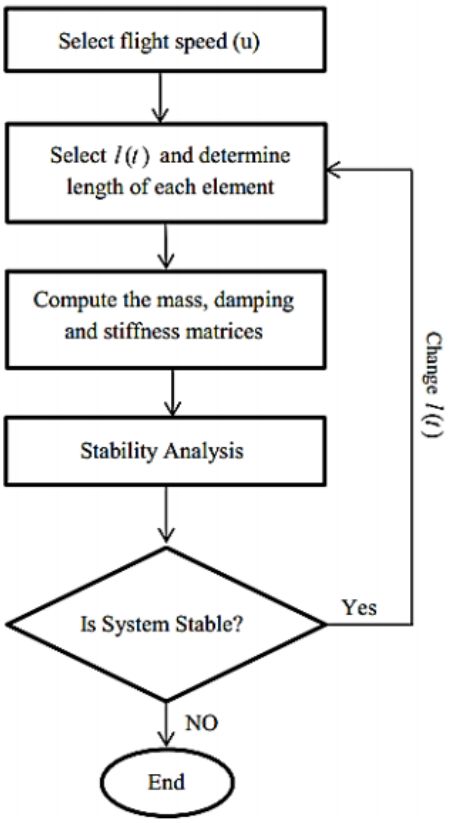

Fig. 3 Flowchart of eigenvalue analysis for the two stage morphing wing

$$[\mathbf{M}]\{\ddot{\mathbf{X}}\} + [\mathbf{C}]\{\dot{\mathbf{X}}\} + [\mathbf{K}]\{\mathbf{X}\} = \{\mathbf{F}\} \tag{10}$$

where **K**, **C** and **M** are the stiffness, mass and damping matrices, respectively.

It is worth mentioning that the above general aeroelastic equations form contains the effects of change in length and related parameters (such as morphing speed). The dynamic instability onset of the system can be found at any time during the length change (step-by-step manner) by assuming the system morphs slowly, employing the eigenvalue analysis (frequency and damping changes with changes in length). This is referred to as the length-based analysis of stability (Moravej Barzani *et al.* 2022b) which can be closer to the actual operation. Fig. 3 shows the flowchart of eigenvalue analysis for the two stage morphing wing. Also, It should be noted that the number of finite elements is fixed in time, and hence the elements size on the moving part changes at each step of time.

3. Verification

To verify the developed model for morphing wings (like as the verification carried out by Moravej Barzani *et al.* (2022b), first the time response of a two-stage Euler-Bernoulli telescopic beam subjected to a concentrated moving mass is obtained and compared with those reported by

Table 1 Parameters of telescopic beams

Parameter	Value
l (m)	10.7
l_m (m)	10.7
m_1 (kg/m)	85
m_2 (kg/m)	46
EI_1 (Nm^2)	35
EI_2 (Nm^2)	35
$\dot{\kappa}$ (m/s)	0.5
m_p (kg)	400

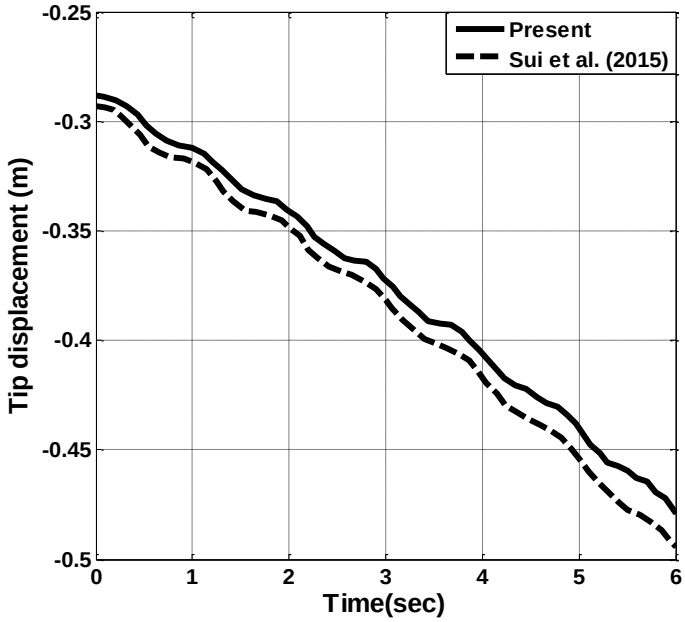

Fig. 4 The dynamic response of a two-stage telescopic beam subjected to a concentrated mass

Sui *et al.* (2015), and shown in Fig. 4. The parameters used for this case are presented in Table. 1. It is clear that the present results are in a good agreement with those presented by Sui *et al.* (2015) with maximum difference of 4%. It is noted that the initial conditions are considered as compatible deformation with the presence of a concentrated mass (m_p) at the end of the beam. Furthermore, here the effect of gravity is retained in the equations to be able to compare the results directly.

Next, to verify the developed model for flutter analysis with rigid-body motion, the work done by Goland and Luke (1948) is considered with the properties presented in Lottati (1987) work. It is noted that Lottati (1987) has used generalized Euler-Bernoulli beam structural model for composite wings and Theodorsen's unsteady aerodynamic model.

Table 2 and Table 3 compare the values of the speed and frequency of flutter obtained from the present analysis with the results presented by Lottati (1987), respectively. It is clear that the present results are in a very good agreement with those presented by Lottati.

Table 2 Validation and comparison of flutter speed under rigid-body condition

	Lottati (1987)	Present method		Percent of Difference
		10 elements	20 elements	
$u_{flutter_1}(ft/s)$	645.4	671.9	669.8	3.8
$u_{flutter_2}(ft/s)$ (Rigid Body Mode)	939	936.3	941.1	0.2

Table 3 Validation and comparison of flutter frequency under rigid-body condition

	Lottati (1987)	Present method		Percent of Difference
		10 elements	20 elements	
$Freq_{flutter_1}(rad/s)$	32.6	30.8	31	4.9
$Freq_{flutter_2}(rad/s)$ (Rigid Body Mode)	14.2	14.3	14.3	0.7

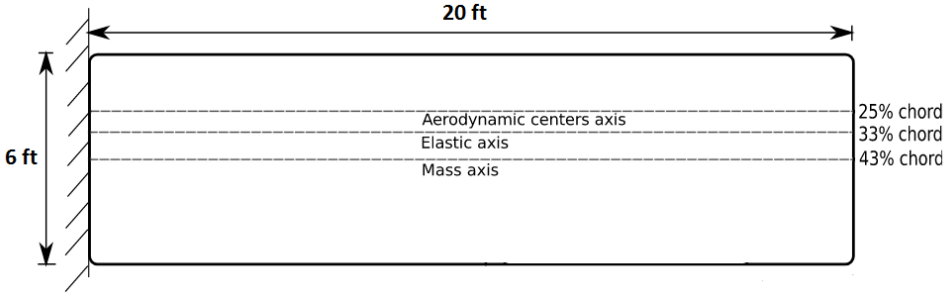

Fig. 5 Goland wing

Table 4 The properties of Goland wing

Parameter	Value
l (ft)	20
c (ft)	6
m (slugs/ft)	0.746
EI_{spanwise} (Lb. ft^2)	23.65×10^6
GJ (Lb. ft^2)	2.39×10^6
Spanwise elastic axis	33% chord
Center of gravity	43% chord
Radius of gyration of wing about mass center	25% chord

It should be noted that in order to present the results, the Goland wing (Fig. 5) is considered with the properties presented in Table 4. Also, for validation, the flutter speed and frequency of this wing are compared with those calculated by Patil (1999) with the clamped boundary condition (Table 5). It is noted that Patil considered this problem by solving the mixed beam formulation using a finite element approach. It is clear that the present results are in very good agreement with those presented by Patil with a maximum difference of 1.6%.

Table 5 The comparison of the flutter speed and frequency of the Goland wing

	Patil (1999)	Present method		Percent of Difference
		10 elements	20 elements	
$u_f(\mathrm{ft/s})$	445	453	452.1	1.6
$\omega_f(\mathrm{rad/s})$	70.2	70.1	70.33	0.2

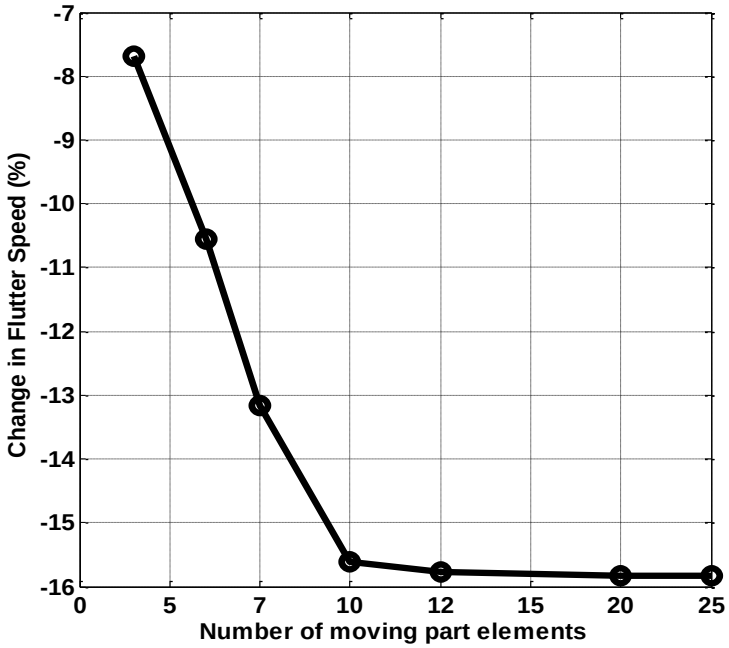

Fig. 6 The convergence of the flutter speed at maximum wing length

In what follows, it is assumed that the Goland wing length due to the moving part in the telescopic wing can be extended up to 50%. Fig. 6 shows the convergence of the flutter speed for the case of maximum length, for different numbers of elements. It is clear that by using 20 elements, the flutter speed can be predicted accurately, and hence from here on, 20 elements are used for moving part (In total, 40 elements are used with the fixed part for all cases).

By considering all above studies, it can be concluded that the developed aeroelastic model is able to capture the flutter stability of telescopic wings with rigid-body motion accurately. In what follows, the effects of various parameters on the aeroelastic stability of telescopic wings with rigid-body motion are investigated. To this aim, the following nondimensional parameters are used

$$M_F = \frac{m_F}{ml_1}$$
$$X_F = \frac{x_F}{b}$$
$$R_F = \frac{r_F}{b}$$
$$\omega_F = \frac{\omega_{\mathrm{Flutter}}}{\omega_\alpha} \tag{11}$$

where ω_α is the first uncoupled torsional frequency.

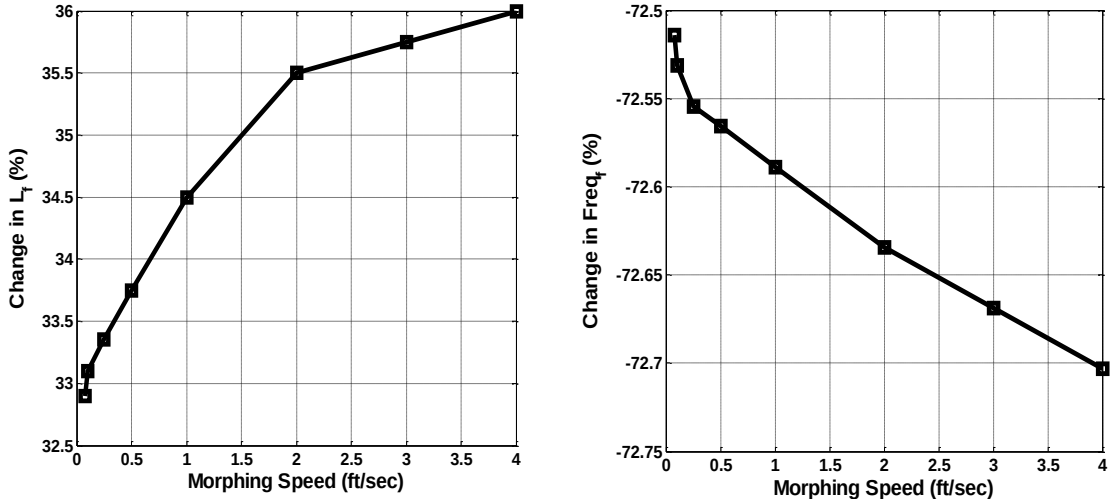

Fig. 7 The effect of morphing speed on the critical length and frequency of the wing ($M_F = 1.34,\ X_F = -1\ ,\ R_F = 2$)

4. Results

In what follows, the critical length, (L_f), at which the wing gets unstable is obtained, and the effects of various parameters with rigid-body condition on the sensitivity of the critical length and its frequency are investigated. It should be noted that the effect of rigid body motion may be a change in the coupling of the modes compared to the case which the wing is analyzed independently with the clamped boundary condition.

4.1 Variation of morphing speed

The effect of morphing speed on the critical length of axially moving wings is determined and shown in Fig. 7. It is noted that unless otherwise stated, from here on all results are presented at a flight speed of 420 ft/s and all values are nondimensionalized (Eq. (11)) using the original wing parameters. Also, all results are presented at a morphing speed ($\dot{\kappa} = 1\ \mathrm{ft/s}$) and the change of flutter mode is written only for non-rigid mode.

Considering the effect of morphing speed results in an improvement of up to 35% in the critical length compared to the original wing. Furthermore, the morphing wing critical length increases (decreases) when the morphing speed increases (decreases). Also, this effect is greater in the small morphing speeds. Moreover, as shown in Fig. 7, the critical frequency of the morphing wing decreases (increases) when the morphing speed increases (decreases). It should be noted that frequencies presented in Fig. 7 are the rigid torsional frequency of the body. Also, the results show that changing the morphing speed does not change the type of flutter mode.

4.2 Variation of flight speed

Obviously, the critical length decreases with increasing flight speed; Also, the critical frequency is increased according to Fig. 8. It is noteworthy that the change of flight speed did not

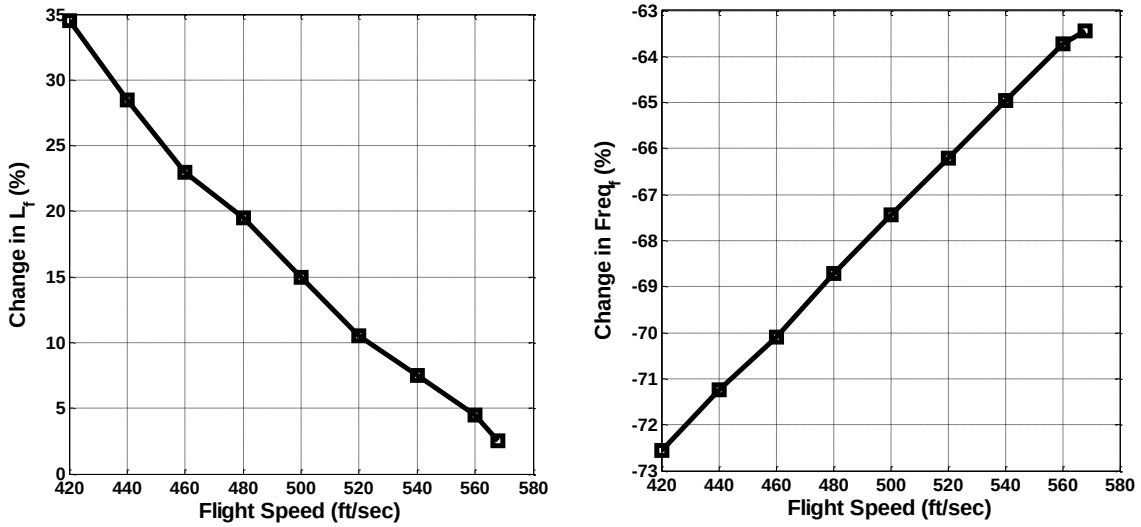

Fig. 8 The effect of flight speed on the critical length and frequency of the wing ($M_F = 1.34,\ X_F = -1,\ R_F = 2$)

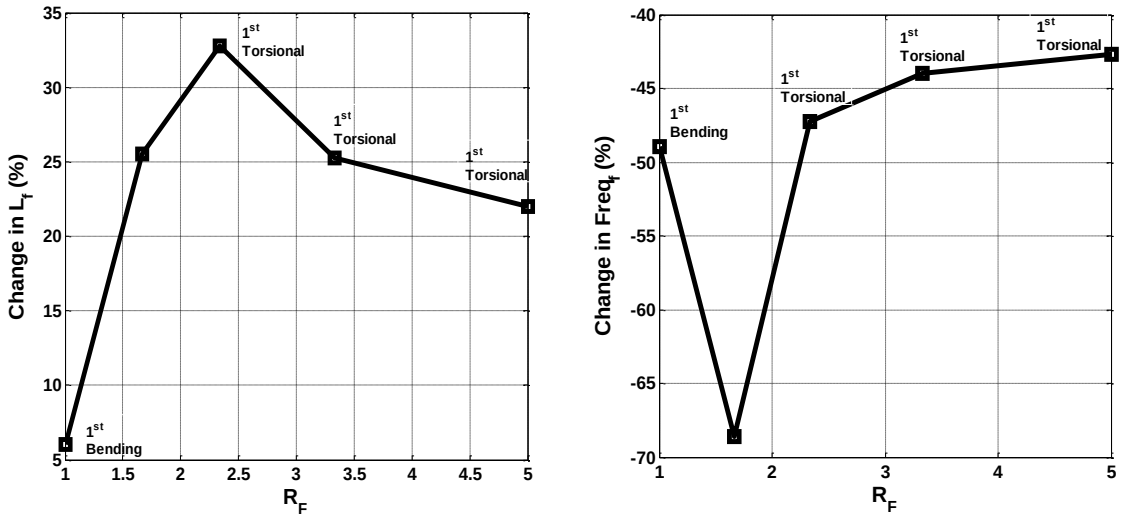

Fig. 9 The effect of radius of gyration on the critical length and frequency of the wing ($M_F = 1.34,\ X_F = -1$)

affect the change of the type of flutter mode and always had a rigid mode (with the mentioned conditions and parameters). Therefore, depending on the parameters studied, the flutter mode may change, but with the change of flight speed, it remains in the same flutter mode.

4.3 Variation of radius of gyration

The effect of fuselage radius of gyration on the critical length is shown in Fig. 9. According to Fig. 9, first the radius of gyration causes the flutter to occur in the first bending mode of the wing

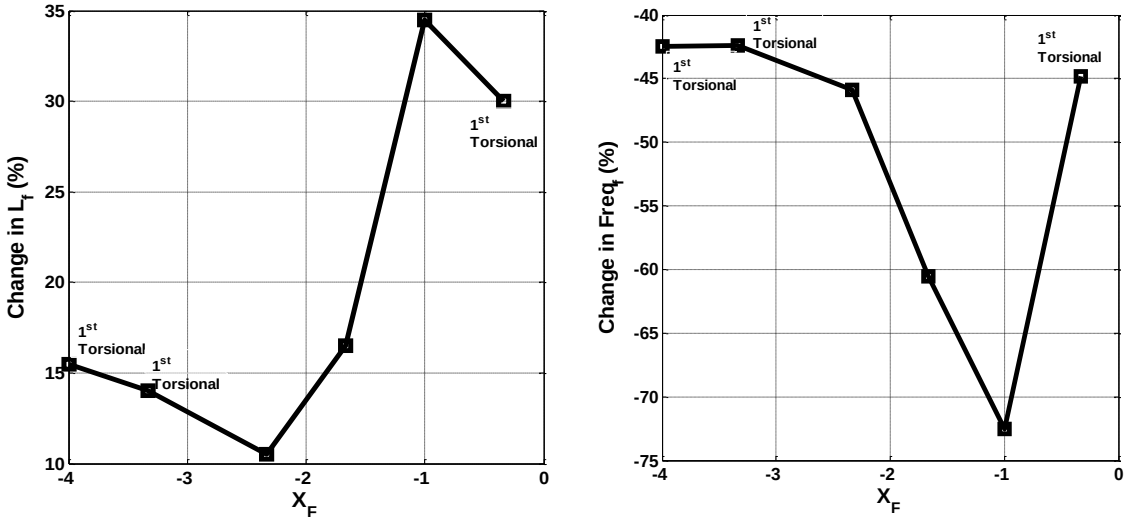

Fig. 10 The effect of fuselage center of gravity distance from wing elastic axis on the critical length and frequency of the wing ($M_F = 1.34,\ R_F = 2$)

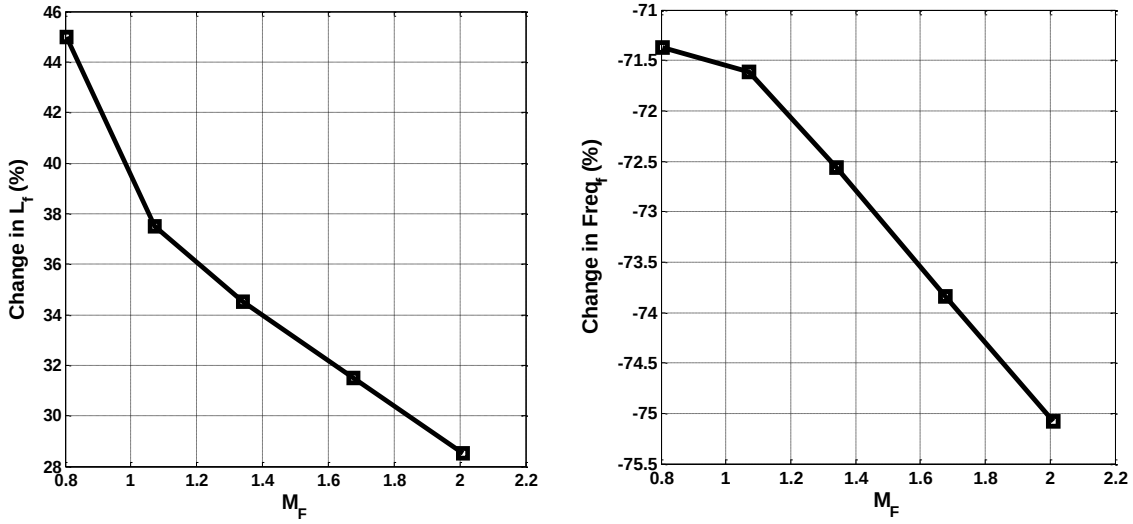

Fig. 11 The effect of fuselage mass on the critical length and frequency of the wing ($X_F = -1,\ R_F = 2$)

(due to the coupling of the first bending mode of the wing with the rigid body mode) and then changed to the rigid body mode (due to the coupling of the first bending mode with the rigid body mode) and by increasing it again, it reaches the torsional mode of the wing (due to the coupling of the first bending and torsional modes of the wing). Also in the present study, it caused a 30% change in critical length. Recent cases indicate the importance and effect of fuselage radius of gyration on the occurrence of flutter. Critical frequency changes can also be seen in Fig. 9. This figure shows up to 25% change in the critical frequency and the fluctuations of the frequencies are due to the change of the critical mode.

4.4 Variation of fuselage center of gravity distance from wing elastic axis

The effect of the distance between the center of gravity of the fuselage and the elastic axis of the wing (body position) on the critical length is shown in Fig. 10. According to Fig. 10, first the fuselage center of gravity distance from wing elastic axis causes the occurrence of a flutter in the first torsional mode of the wing (due to coupling of the first bending and torsional modes of the wing) and then changed to rigid body mode (due to coupling of the first bending mode of the wing with the rigid body mode) and by changing it again reaches the first torsional mode of the wing (coupling of the first bending and torsional modes of the wing). Also in the present study, the difference in critical length values with increasing the fuselage center of gravity distance from the wing elastic axis is up to 25%, which indicates the importance of this parameter. The critical frequency changes can also be seen in Fig. 10. This figure shows up to 30% change in critical frequency and the fluctuation of frequencies is due to changes in the critical mode. Like the radius of gyration, the fuselage center of gravity distance from wing elastic axis can cause unpredictable changes in the critical length and frequency; Therefore, paying attention to these parameters and how to change them will be of special importance in structural design process.

4.5 Variation of fuselage mass

Fig. 11 shows the effect of fuselage mass on the critical length. According to Fig. 11, it can be seen that with increasing (decreasing) fuselage mass, the critical length decreases (increases) and this parameter is inversely related to the critical length. Also, in the present study, all critical modes have occurred in the rigid body mode. Of course, with the change of other parameters, another mode may become critical, but what is observed indicates that the fuselage mass parameter has no effect on changing the type of critical mode. The critical frequency variations are also shown in Fig. 11. This figure shows that the critical frequency is inversely related to the fuselage mass, and an increase (decrease) in fuselage mass causes a decrease (increase) in the critical frequency.

5. Conclusions

In this study, the effects of rigid-body motion on the aeroelastic stability of a two-stage axially deploying telescopic wing have been studied. The extended Hamilton's principle has been used to derive the equations of motion. The equations have been discretized with finite element method. Validation of the results is obtained by comparing with those available in the literature. The effect of rigid-body parameters on the wing stability has been determined by checking the system eigenvalues. A summary of the results of this study is as follows:

1. The variation of the morphing speed, flight speed and fuselage mass has no effect on changing the type of flutter mode.
2. The critical length and frequency are inversely related to the fuselage mass and their sensitivity to changing this parameter is low.
3. The critical length and frequency are more sensitive to the radius of gyration and the fuselage center of gravity distance from wing elastic axis, and these two parameters can cause unpredictable changes in the critical length and frequency.
4. Paying attention to the fuselage parameters and how they affect stability is very important

and will play a significant role in the design.

Declaration of conflicting interests

The authors declared no potential conflicts of interest with respect to the research, authorship, and/or publication of this article.

References

Ajaj, R.M. and Friswell, M.I. (2018), "Aeroelasticity of compliant span morphing wings", *Smart Mater. Struct.*, **27**(10), 105052. https://doi.org/10.1088/1361-665X/aad219.

Ajaj, R.M., Omar, F.K., Darabseh, T.T. and Cooper, J. (2019), "Flutter of telescopic span morphing wings", *Int. J. Struct. Stab. Dyn.*, **19**(06), 1950061. https://doi.org/10.1142/S0219455419500615.

Bisplinghoff, R.L., Ashley, H. and Halfman, R.L. (2013), *Aeroelasticity*, Courier Corporation.

Chang, J.R., Lin, W.J., Huang, C.J. and Choi, S.T. (2010), "Vibration and stability of an axially moving Rayleigh beam", *Appl. Math. Model.*, **34**(6), 1482-1497. https://doi.org/10.1016/j.apm.2009.08.022.

Cook, R.D. (2007), *Concepts and Applications of Finite Element Analysis*, John wiley & sons.

Duan, Y.C., Wang, J.P., Wang, J.Q., Liu, Y.W. and Shao, F. (2014), "Theoretical and experimental study on the transverse vibration properties of an axially moving nested cantilever beam", *J. Sound Vib.*, **333**(13), 2885-2897. https://doi.org/10.1016/j.jsv.2014.02.021.

Friswell, M.I. and Inman, D.J. (2006), "Morphing concepts for UAVs", *21st Bristol UAV Systems Conference*, April.

Goland, M. and Luke, Y.L. (1948), "The flutter of a uniform wing with tip weights", 13-20.

Huang, C., Chao, Y.A.N.G., Zhigang, W.U. and Changhong, T.A.N.G. (2018), "Variations of flutter mechanism of a span-morphing wing involving rigid-body motions", *Chin. J. Aeronaut.*, **31**(3), 490-497. https://doi.org/10.1016/j.cja.2017.12.014.

Huang, R. and Qiu, Z. (2013), "Transient aeroelastic responses and flutter analysis of a variable-span wing during the morphing process", *Chin. J. Aeronaut.*, **26**(6), 1430-1438. https://doi.org/10.1016/j.cja.2013.07.047.

Li, W. and Jin, D. (2018), "Flutter suppression and stability analysis for a variable-span wing via morphing technology", *J. Sound Vib.*, **412**, 410-423. https://doi.org/10.1016/j.jsv.2017.10.009.

Lottati, I. (1987), "Aeroelastic stability characteristics of a composite swept wing withtip weights for an unrestrained vehicle", *J. Aircraft*, **24**(11), 793-802. https://doi.org/10.2514/3.45523.

Moravej Barzani, S.H., Shahverdi, H. and Amoozgar, M. (2022), "Nonlinear aeroelastic stability analysis of a two-stage axially moving telescopic wing by using fully intrinsic equations", *Proc. Inst. Mech. Eng., Part G: J. Aerosp. Eng.*, **236**(15), 3102-3110. https://doi.org/10.1177/09544100221080117.

Moravej Barzani, S.H., Shahverdi, H. and Amoozgar, M. (2023), "Parametric study on the dynamic aeroelastic analysis of a two-stage axially deploying telescopic wing", *J. Vib. Control*, **29**(9-10), 2021-2034. https://doi.org/10.1177/10775463221074145.

Park, S., Yoo, H.H. and Chung, J. (2013), "Vibrations of an axially moving beam with deployment or retraction", *AIAA J.*, **51**(3), 686-696. https://doi.org/10.2514/1.J052059.

Patil, M.J. (1999), *Nonlinear Aeroelastic Analysis, Flight Dynamics, and Control of a Complete Aircraft*, Georgia Institute of Technology.

Peters, D.A., Karunamoorthy, S. and Cao, W.M. (1995), "Finite state induced flow models. I-Two-dimensional thin airfoil", *J. Aircraft*, **32**(2), 313-322. https://doi.org/10.2514/3.46718.

Raftoyiannis, I.G. and Michaltsos, G.T. (2013), "Dynamic behavior of telescopic cranes boom", *Int. J. Struct. Stab. Dyn.*, **13**(01), 1350010. https://doi.org/10.1142/S0219455413500107.

Salami, S.J. and Dariushi, S. (2018), "Geometrically nonlinear analysis of sandwich beams under low velocity impact: analytical and experimental investigation", *Steel Compos. Struct*., **27**(3), 273-283. https://doi.org/10.12989/scs.2018.27.3.273.

Schmidt, D.K., Zhao, W. and Kapania, R.K. (2016), "Flight-dynamics and flutter modeling and analyses of a flexible flying-wing drone-invited", *AIAA Atmospheric Flight Mechanics Conference*, 1748. https://doi.org/10.2514/6.2016-1748.

Shafaghat, S., Noorian, M.A. and Irani, S. (2022), "Nonlinear aeroelastic analysis of a HALE aircraft with flexible components", *Aerosp. Sci. Technol.*, **127**, 107663. https://doi.org/10.1016/j.ast.2022.107663.

Stylianou, M. and Tabarrok, B. (1994a), "Finite element analysis of an axially moving beam, part I: time integration", *J. Sound Vib.*, **178**(4), 433-453. https://doi.org/10.1006/jsvi.1994.1497.

Sui, W., Zhu, Z. and Cao, G. (2016), "Dynamic responses of axially moving telescopic mechanism for truss structure bridge inspection vehicle under moving mass", *J. Vibroeng.*, **18**(1), 408-416.

Sui, W., Zhu, Z., Cao, G. and Chen, G. (2016), "Dynamic behaviors of 2-DOF axially telescopic mechanism for truss structure bridge inspection vehicle", *J. Vibroeng.*, **18**(2), 1145-1156. https://doi.org/10.21595/jve.2016.16436.

Wang, P.K.C. and Wei, J.D. (1987), "Vibrations in a moving flexible robot arm", *J. Sound Vib.*, **116**(1), 149-160. https://doi.org/10.1016/S0022-460X(87)81326-3.

Yang, X.D. and Zhang, W. (2014), "Nonlinear dynamics of axially moving beam with coupled longitudinal–transversal vibrations", *Nonlin. Dyn.*, **78**, 2547-2556. https://doi.org/10.1007/s11071-014-1609-5.

Yang, X.D., Zhang, W. and Melnik, R.V. (2016), "Energetics and invariants of axially deploying beam with uniform velocity", *AIAA J.*, **54**(7), 2183-2189. https://doi.org/10.2514/1.J054383.

Zhang, W., Lu, S.F. and Yang, X.D. (2014), "Analysis on nonlinear dynamics of a deploying composite laminated cantilever plate", *Nonlin. Dyn.*, **76**, 69-93. https://doi.org/10.1007/s11071-013-1111-5.

Zhang, W., Chen, L.L., Guo, X.Y. and Sun, L. (2017), "Nonlinear dynamical behaviors of deploying wings in subsonic air flow", *J. Fluid. Struct.*, **74**, 340-355. https://doi.org/10.1016/j.jfluidstructs.2017.04.006.

AP

Appendix A

substituting Eq. (7) in Eq. (6) results in Eq. (A.1)

$$\left.\begin{aligned}&\left(m_1+m_e\delta(x-l_1)\right)\left[\frac{d^2h_1}{dt^2}+g\right]+m_1r_1\frac{d^2\alpha_1}{dt^2}+\frac{d^2}{dx^2}\left(EI_1\frac{d^2h_1}{dx^2}\right)=L\\&I_{e.c_1}\frac{d^2\alpha_1}{dt^2}+m_er_1\delta(x-l_1)\frac{d^2\alpha_1}{dt^2}+m_1r_1\frac{d^2h_1}{dt^2}-\frac{d}{dx}\left(GJ_1\frac{d\alpha_1}{dx}\right)+m_1r_1g=M_{e.c}\end{aligned}\right\}\ 0<x<l_1$$

$$\left.\begin{aligned}&m_2\left(\frac{\partial^2h_2}{\partial t^2}+2\dot\kappa\frac{\partial^2h_2}{\partial x\partial t}+\dot\kappa^2\frac{\partial^2h_2}{\partial x^2}+\ddot\kappa\frac{\partial h_2}{\partial x}+g\right)+\\&+m_2r_2\left(\frac{\partial^2\alpha_2}{\partial t^2}+2\dot\kappa\frac{\partial^2\alpha_2}{\partial x\partial t}+\dot\kappa^2\frac{\partial^2\alpha_2}{\partial x^2}+\ddot\kappa\frac{\partial\alpha_2}{\partial x}\right)+\frac{d^2}{dx^2}\left(EI_2\frac{d^2h_2}{dx^2}\right)=L\\&I_{e.c_2}\left(\frac{\partial^2\alpha_2}{\partial t^2}+2\dot\kappa\frac{\partial^2\alpha_2}{\partial x\partial t}+\dot\kappa^2\frac{\partial^2\alpha_2}{\partial x^2}+\ddot\kappa\frac{\partial\alpha_2}{\partial x}\right)+\\&+m_2r_2\left(\frac{\partial^2h_2}{\partial t^2}+2\dot\kappa\frac{\partial^2h_2}{\partial x\partial t}+\dot\kappa^2\frac{\partial^2h_2}{\partial x^2}+\ddot\kappa\frac{\partial h_2}{\partial x}\right)-\frac{d}{dx}\left(GJ_2\frac{d\alpha_2}{dx}\right)+m_2r_2g=M_{e.c}\end{aligned}\right\}\ l_1<x<l \quad \text{(A.1)}$$

The weak form of Eq. (A.1) is obtained as (A.2) (Moravej Barzani *et al.* 2022b).
Fixed part ($\dot\kappa=0,\ddot\kappa=0$):

$$\sum_{j=1}^{n_1}\Big[m_{ij}^a\ddot h_j+rm_{ij}^b\ddot\alpha_j+2\big(c_{ij}^a+\dot\kappa c_{ij}^b\big)\dot h_j+2r\big(c_{ij}^c+\dot\kappa c_{ij}^d\big)\dot\alpha_j+\big(k_{ij}^a+2\dot\kappa k_{ij}^b+\dot\kappa^2k_{ij}^c+\ddot\kappa k_{ij}^d+k_{ij}^e\big)h_j+r\Big(k_{ij}^f+2\dot\kappa k_{ij}^g+\dot\kappa^2k_{ij}^h+\ddot\kappa k_{ij}^k\Big)\alpha_j+f_i^g+m_{ij}^c\ddot\psi_j+m_{ij}^d\ddot\varphi_j\Big]=L^g$$

$$\sum_{n=1}^{n_1}\Big[rm_{mn}^a\ddot h_n+m_{mn}^b\ddot\alpha_n+2r\big(c_{mn}^a+\dot\kappa c_{mn}^b\big)\dot h_n+2\big(c_{mn}^c+\dot\kappa c_{mn}^d\big)\dot\alpha_n+r\big(k_{mn}^a+2\dot\kappa k_{mn}^b+\dot\kappa^2k_{mn}^c+\ddot\kappa k_{mn}^d\big)h_n+\big(k_{mn}^f+2\dot\kappa k_{mn}^g+\dot\kappa^2k_{mn}^o+\ddot\kappa k_{mn}^p-k_{mn}^e\big)\alpha_n+rf_m^g+m_{mn}^c\ddot\psi_n+m_{mn}^d\ddot\varphi_n\Big]=M_{e.c}^g$$

Moving part

$$\sum_{j=n_1+1}^{N}\Big[m_{ij}^a\ddot h_j+rm_{ij}^b\ddot\alpha_j+2\big(c_{ij}^a+\dot\kappa c_{ij}^b\big)\dot h_j+2r\big(c_{ij}^c+\dot\kappa c_{ij}^d\big)\dot\alpha_j+\big(k_{ij}^a+2\dot\kappa k_{ij}^b+\dot\kappa^2k_{ij}^c+\ddot\kappa k_{ij}^d+k_{ij}^e\big)h_j+r\Big(k_{ij}^f+2\dot\kappa k_{ij}^g+\dot\kappa^2k_{ij}^h+\ddot\kappa k_{ij}^k\Big)\alpha_j+f_i^g\Big]=L^g$$

$$\sum_{n=n_1+1}^{N}\Big[rm_{mn}^a\ddot h_n+m_{mn}^b\ddot\alpha_n+2r\big(c_{mn}^a+\dot\kappa c_{mn}^b\big)\dot h_n+2\big(c_{mn}^c+\dot\kappa c_{mn}^d\big)\dot\alpha_n+r\big(k_{mn}^a+2\dot\kappa k_{mn}^b+\dot\kappa^2k_{mn}^c+\ddot\kappa k_{mn}^d\big)h_n+\big(k_{mn}^f+2\dot\kappa k_{mn}^g+\dot\kappa^2k_{mn}^o+\ddot\kappa k_{mn}^p-k_{mn}^e\big)\alpha_n+rf_m^g\Big]=M_{e.c}^{\ g} \quad \text{(A.2)}$$

Also, the weak form of aerodynamic equations can be written as

$$L^g=\sum_{j=1}^{n}\Big\{\pi\rho b^2\Big[m_{ij}^c\ddot h_j-bam_{ij}^d\ddot\alpha_j+2\Big(c_{ij}^e+\dot\kappa c_{ij}^f\Big)\dot h_j-2ba\Big(c_{ij}^g+\dot\kappa c_{ij}^p\Big)\dot\alpha_j+uc_{ij}^q\dot\alpha_j+\Big(k_{ij}^l+2\dot\kappa k_{ij}^o+\dot\kappa^2k_{ij}^p+\ddot\kappa k_{ij}^q\Big)h_j-ba\big(k_{ij}^r+2\dot\kappa k_{ij}^s+\dot\kappa^2k_{ij}^t+\ddot\kappa k_{ij}^u\big)\alpha_j+u(k_{ij}^v+k_{ij}^w)\alpha_j\Big]+2\pi\rho ub[c_{ij}^r\dot h_j+b\left(\tfrac{1}{2}-a\right)c_{ij}^q\dot\alpha_j+(k_{ij}^y+k_{ij}^z)h_j+uk_{ij}^x\alpha_j+b(\tfrac{1}{2}-a)(k_{ij}^v+k_{ij}^w)\alpha_j-\lambda_0]\Big\}$$

$$M_{c/4}^g=-\pi\rho b^3\sum_{n=1}^{N}\Big\{\frac{1}{2}m_{mn}^c\ddot h_n+b\left(\frac{1}{8}-\frac{a}{2}\right)m_{mn}^d\ddot\alpha_n+\big(c_{mn}^e+\dot\kappa c_{mn}^f\big)\dot h_n+b\left(\frac{1}{4}-a\right)\big(c_{mn}^g+\dot\kappa c_{mn}^p\big)\dot\alpha_n+uc_{mn}^q\dot\alpha_n+\frac{1}{2}\big(k_{mn}^l+2\dot\kappa k_{mn}^o+\dot\kappa^2k_{mn}^p+\ddot\kappa k_{mn}^q\big)h_n+b(\tfrac{1}{8}-\tfrac{a}{2})(k_{mn}^r+2\dot\kappa k_{mn}^s+\dot\kappa^2k_{mn}^t+\ddot\kappa k_{mn}^u)\alpha_n+u(k_{mn}^v+k_{mn}^w)\alpha_n\Big\} \quad \text{(A.3)}$$

Appendix B

Considering torsional and bending shape functions ($H^{\alpha}(x)$ and $H^{h}(x)$), the related matrices are introduced as follows

$$m_{ij}^{a}=m\int_{x_j}^{x_{j+1}}H_i^h H_j^h dx \qquad m_{mn}^{a}=m\int_{x_n}^{x_{n+1}}H_m^{\alpha} H_n^h dx \qquad m_{ij}^{c}=\int_{x_j}^{x_{j+1}}H_i^h H_j^h dx \qquad m_{mn}^{c}=\int_{x_n}^{x_{n+1}}H_m^{\alpha} H_n^h dx$$

$$c_{ij}^{a}=m\int_{x_j}^{x_{j+1}}H_i^h \dot{H}_j^h dx \qquad c_{mn}^{a}=m\int_{x_n}^{x_{n+1}}H_m^{\alpha} \dot{H}_n^h dx \qquad c_{ij}^{e}=\int_{x_j}^{x_{j+1}}H_i^h \dot{H}_j^h dx \qquad c_{mn}^{e}=\int_{x_n}^{x_{n+1}}H_m^{\alpha} \dot{H}_n^h dx$$

$$c_{ij}^{b}=m\int_{x_j}^{x_{j+1}}H_i^h H'^h_j dx \qquad c_{mn}^{b}=m\int_{x_n}^{x_{n+1}}H_m^{\alpha} H'^h_n dx \qquad c_{ij}^{f}=\int_{x_j}^{x_{j+1}}H_i^h H'^h_j dx \qquad c_{mn}^{f}=\int_{x_n}^{x_{n+1}}H_m^{\alpha} H'^h_n dx$$

$$k_{ij}^{a}=m\int_{x_j}^{x_{j+1}}H_i^h \ddot{H}_j^h dx \qquad k_{mn}^{a}=m\int_{x_n}^{x_{n+1}}H_m^{\alpha} \ddot{H}_n^h dx \qquad k_{ij}^{l}=\int_{x_j}^{x_{j+1}}H_i^h \ddot{H}_j^h dx \qquad k_{mn}^{l}=\int_{x_n}^{x_{n+1}}H_m^{\alpha} \ddot{H}_n^h dx$$

$$k_{ij}^{b}=m\int_{x_j}^{x_{j+1}}H_i^h \dot{H}'^h_j dx \qquad k_{mn}^{b}=m\int_{x_n}^{x_{n+1}}H_m^{\alpha} \dot{H}'^h_n dx \qquad k_{ij}^{o}=\int_{x_j}^{x_{j+1}}H_i^h \dot{H}'^h_j dx \qquad k_{mn}^{o}=\int_{x_n}^{x_{n+1}}H_m^{\alpha} \dot{H}'^h_n dx$$

$$k_{ij}^{c}=m\int_{x_j}^{x_{j+1}}H_i^h H''^h_j dx \qquad k_{mn}^{c}=m\int_{x_n}^{x_{n+1}}H_m^{\alpha} H''^h_n dx \qquad k_{ij}^{p}=\int_{x_j}^{x_{j+1}}H_i^h H''^h_j dx \qquad k_{mn}^{p}=\int_{x_n}^{x_{n+1}}H_m^{\alpha} H''^h_n dx$$

$$k_{ij}^{d}=m\int_{x_j}^{x_{j+1}}H_i^h H'^h_j dx \qquad k_{mn}^{d}=m\int_{x_n}^{x_{n+1}}H_m^{\alpha} H'^h_n dx \qquad k_{ij}^{q}=\int_{x_j}^{x_{j+1}}H_i^h H'^h_j dx \qquad k_{mn}^{q}=\int_{x_n}^{x_{n+1}}H_m^{\alpha} H'^h_n dx$$

$$m_{ij}^{b}=m\int_{x_j}^{x_{j+1}}H_i^h H_j^{\alpha} dx \qquad m_{mn}^{b}=I_{e.c}\int_{x_n}^{x_{n+1}}H_m^{\alpha} H_n^{\alpha} dx \qquad m_{ij}^{d}=\int_{x_j}^{x_{j+1}}H_i^h H_j^{\alpha} dx \qquad m_{mn}^{d}=\int_{x_n}^{x_{n+1}}H_m^{\alpha} H_n^{\alpha} dx$$

$$c_{ij}^{c}=m\int_{x_j}^{x_{j+1}}H_i^h \dot{H}_j^{\alpha} dx \qquad c_{mn}^{c}=I_{e.c}\int_{x_n}^{x_{n+1}}H_m^{\alpha} \dot{H}_n^{\alpha} dx \qquad c_{ij}^{g}=\int_{x_j}^{x_{j+1}}H_i^h \dot{H}_j^{\alpha} dx \qquad c_{mn}^{g}=\int_{x_n}^{x_{n+1}}H_m^{\alpha} \dot{H}_n^{\alpha} dx$$

$$c_{ij}^{d}=m\int_{x_j}^{x_{j+1}}H_i^h H'^{\alpha}_j dx \qquad c_{mn}^{d}=I_{e.c}\int_{x_n}^{x_{n+1}}H_m^{\alpha} H'^{\alpha}_n dx \qquad c_{ij}^{p}=\int_{x_j}^{x_{j+1}}H_i^h H'^{\alpha}_j dx \qquad c_{mn}^{p}=\int_{x_n}^{x_{n+1}}H_m^{\alpha} H'^{\alpha}_n dx$$

$$k_{ij}^{f}=m\int_{x_j}^{x_{j+1}}H_i^h \ddot{H}_j^{\alpha} dx \qquad k_{mn}^{f}=I_{e.c}\int_{x_n}^{x_{n+1}}H_m^{\alpha} \ddot{H}_n^{\alpha} dx \qquad c_{ij}^{q}=\int_{x_j}^{x_{j+1}}H_i^h H_j^{\alpha} dx \qquad c_{mn}^{q}=\int_{x_n}^{x_{n+1}}H_m^{\alpha} H_n^{\alpha} dx$$

$$k_{ij}^{g}=m\int_{x_j}^{x_{j+1}}H_i^h \dot{H}'^{\alpha}_j dx \qquad k_{mn}^{g}=I_{e.c}\int_{x_n}^{x_{n+1}}H_m^{\alpha} \dot{H}'^{\alpha}_n dx \qquad c_{ij}^{r}=\int_{x_j}^{x_{j+1}}H_i^h H_j^h dx \qquad k_{mn}^{r}=\int_{x_n}^{x_{n+1}}H_m^{\alpha} \ddot{H}_n^{\alpha} dx$$

$$k_{ij}^{h}=m\int_{x_j}^{x_{j+1}}H_i^h H''^{\alpha}_j dx \qquad k_{mn}^{o}=I_{e.c}\int_{x_n}^{x_{n+1}}H_m^{\alpha} H''^{\alpha}_n dx \qquad k_{ij}^{r}=\int_{x_j}^{x_{j+1}}H_i^h \ddot{H}_j^{\alpha} dx \qquad k_{mn}^{s}=\int_{x_n}^{x_{n+1}}H_m^{\alpha} \dot{H}'^{\alpha}_n dx$$

$$k_{ij}^{k}=m\int_{x_j}^{x_{j+1}}H_i^h H'^{\alpha}_j dx \qquad k_{mn}^{p}=I_{e.c}\int_{x_n}^{x_{n+1}}H_m^{\alpha} H'^{\alpha}_n dx \qquad k_{ij}^{s}=\int_{x_j}^{x_{j+1}}H_i^h \dot{H}'^{\alpha}_j dx \qquad k_{mn}^{t}=\int_{x_n}^{x_{n+1}}H_m^{\alpha} H''^{\alpha}_n dx$$

$$k_{ij}^{e} = EI\int_{x_j}^{x_{j+1}} H''^{h}_{i} H''^{h}_{j}\,dx \qquad k_{mn}^{e} = GJ\int_{x_n}^{x_{n+1}} H'^{\alpha}_{m} H'^{\alpha}_{n}\,dx \qquad k_{ij}^{t} = \int_{x_j}^{x_{j+1}} H_i^h H''^{\alpha}_{j}\,dx \qquad k_{mn}^{u} = \int_{x_n}^{x_{n+1}} H_m^{\alpha} H'^{\alpha}_{n}\,dx$$

$$f_i^{g} = mg\int_{x_j}^{x_{j+1}} H_i^h\,dx \qquad f_m^{g} = mg\int_{x_n}^{x_{n+1}} H_m^{\alpha}\,dx \qquad k_{ij}^{w} = \int_{x_j}^{x_{j+1}} H_i^h H'^{\alpha}_{j}\,dx \qquad k_{mn}^{w} = \int_{x_n}^{x_{n+1}} H_m^{\alpha} H'^{\alpha}_{n}\,dx$$

$$k_{ij}^{u} = \int_{x_j}^{x_{j+1}} H_i^h H'^{\alpha}_{j}\,dx \qquad k_{mn}^{v} = \int_{x_n}^{x_{n+1}} H_m^{\alpha} \dot{H}_n^{\alpha}\,dx \qquad k_{ij}^{v} = \int_{x_j}^{x_{j+1}} H_i^h \dot{H}_j^{\alpha}\,dx \qquad k_{ij}^{x} = \int_{x_j}^{x_{j+1}} H_i^h H_j^{\alpha}\,dx$$

$$k_{ij}^{y} = \int_{x_j}^{x_{j+1}} H_i^h \dot{H}_j^h\,dx \qquad k_{ij}^{z} = \int_{x_j}^{x_{j+1}} H_i^h H'^{h}_{j}\,dx \qquad m_{ij}^{c} = m_F\int_{x_j}^{x_{j+1}} H_i^h H_j^h\,dx \qquad m_{ij}^{d} = m_F x_F\int_{x_j}^{x_{j+1}} H_i^h H_j^{\alpha}\,dx$$

$$m_{mn}^{c} = m_F x_F\int_{x_n}^{x_{n+1}} H_m^{\alpha} H_n^h\,dx \qquad m_{mn}^{d} = m_F r_F^2\int_{x_n}^{x_{n+1}} H_m^{\alpha} H_n^{\alpha}\,dx$$